JOURNAL OF AIRCRAFT
Vol. 47, No. 6, November–December 2010

Targeted Energy Transfer Between a Model Flexible Wing and Nonlinear Energy Sink

Sean A. Hubbard,* D. Michael McFarland,† Lawrence A. Bergman,‡ and Alexander F. Vakakis§
University of Illinois at Urbana–Champaign, Urbana, Illinois 61801

DOI: 10.2514/1.C001012

Passive and nonlinear targeted energy transfers induced by resonant interactions between a single-degree-of-freedom nonlinear energy sink and a flexible swept wing are studied. With a series of ground-vibration tests, it is shown that the nonlinear energy sink can be designed to quickly and efficiently absorb energy from one or more wing modes in a completely passive manner. Results indicate that it is feasible to use such a device to suppress or prevent aeroelastic instabilities like limit-cycle oscillations. The design of a compact nonlinear energy sink is introduced and the parameters of the device are examined experimentally, confirming that the required nonlinearizable stiffness is achieved. Ground-vibration experiments performed on the wing's nonlinear energy-sink system indicate that targeted energy transfer is achievable, resulting in a significant reduction in the second bending mode response of the wing. Furthermore, a finite element model of the system is developed to computationally reproduce the experiments, providing good agreement between the two. Finally, the finite element model is used to simulate the effects of increased nonlinear energy-sink stiffness on the system and to show the conditions under which the nonlinear energy sink will resonantly interact with higher-frequency wing modes.

I. Introduction

MITIGATION of unwanted vibrations in flexible structures is an important design consideration in many fields of engineering. This is especially true in aerospace engineering, where lightweight, flexible structures are desirable. The design of aircraft must consider complex dynamic interactions between the fluid, through which the vehicle travels, and the flexible structure. Especially for high-performance vehicles, this fluid–structure interaction can give rise to instabilities or large-amplitude vibrations that, in the extreme case, may lead to catastrophic failure.

Under normal flight conditions for most aircraft, a dynamic perturbation either to the aircraft structure or to the surrounding airflow will initiate some vibration, which will be dissipated given enough time. However, under certain circumstances the dynamic loading on the vehicle may become synchronized with the response to the perturbation, leading to unstable vibrations that grow unbounded in amplitude. This instability is often referred to as aeroelastic flutter. More often, though, the response of the structure is limited by structural or other nonlinearities resulting in limit-cycle oscillations (LCOs). Nonetheless, LCOs are undesirable for a number of reasons, including structural fatigue and the limitations that they impose on aircraft performance and maneuverability; so, efforts are made to avoid them.

Currently, there are few strategies to address the problem of suppressing LCOs in aircraft. The most common uses flight tests to determine the conditions under which a particular aircraft is likely to experience LCOs and then limits the operation of the vehicle to maneuvers that are not likely to trigger instabilities. This is generally acceptable for private and commercial aircraft. However, for high-performance vehicles found in military applications, this option becomes time-consuming and costly, especially as new external store configurations become available. Numerous methods have been proposed to make aircraft more resistant to LCOs, ranging from gross structural changes (usually prohibitively difficult and expensive) to active control using existing or retrofitted flight control systems. The active control methods in particular have attracted researchers' attention, and several have been shown to have potential to improve stability (see, e.g., [1–3]). Unfortunately, active controls add significant mass to the aircraft and are a potential source of instability. Furthermore, the cost and complexity of such systems would likely be significant.

As an alternative to the aforementioned options, recent work has been directed toward nonlinear targeted energy transfer (TET) [4–7] as a method to mitigate, or even prevent, LCOs in a completely passive manner [8–11]. TET is achieved by the nearly irreversible transfer of broadband energy from the primary structure (in this case the wing of an aircraft) to a lightweight attachment with essentially nonlinear stiffness, the nonlinear energy sink (NES), where it is confined and locally dissipated without spreading back to the primary structure. In essence, the NES may be regarded as a passive broadband boundary controller [12]. If this solution is realized in a practical setting, it could eliminate the need for costly flight testing and/or complex and costly controls, and it could expand the operating envelope of high-performance vehicles.

Lee et al. [8,9] studied the unstable aeroelastic dynamics of a rigid, two-degree-of-freedom (2-DOF) wing model with simulations and experiments. Figure 1 shows the schematic of the wing model, including the nonlinear spring attachments to ground, which limit the unstable response of the model so that the LCO can be achieved. It was shown that for the wing without an NES attachment, LCO can be triggered by an initial excitation of the heave mode, but the instability occurs predominantly in the pitch mode [13]. The trigger and LCO development are transient phenomena that involve broadband energy exchange between the flow and the wing, as well as between wing modes. This property of LCOs is well suited to control by TET because of the ability of the NES to quickly dissipate broadband energy in a passive manner. This is enabled by the essentially nonlinear stiffness of the NES, which allows it to resonantly interact with, and affect, wing modes over broad frequency and energy ranges.

When an NES with a pure cubic stiffness was added to the wing at the location shown in Fig. 1, three LCO suppression mechanisms were identified in simulations at particular coefficients of the NES spring and damper, ratio of the NES mass to the wing mass, and

Received 3 November 2009; revision received 1 March 2010; accepted for publication 29 June 2010.

*Graduate Research Assistant, Department of Aerospace Engineering, 104 South Wright Street; hubbard.sean@gmail.com.

†Research Associate Professor, Department of Aerospace Engineering, 104 South Wright Street, dmmcf@illinois.edu; Senior Member AIAA.

‡Professor, Department of Aerospace Engineering, 104 South Wright Street, lbergman@illinois.edu; Associate Fellow AIAA.

§Professor, Department of Mechanical Science and Engineering, 1206 West Green Street; avakakis@illinois.edu.

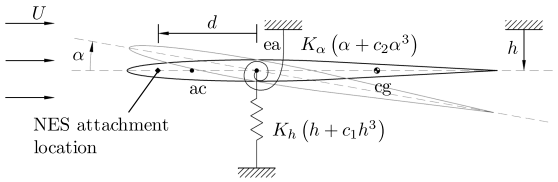

Fig. 1 Schematic of a two-DOF rigid wing in a freestream with velocity *U*, used by Lee et al. [8,9] to study LCOs and TET; features include the center of gravity (cg), elastic axis (ea), aerodynamic center (ac), heave displacement (*h*), pitch angle (α), and an NES attached a distance (*d*), forward of ea.

position of the NES on the wing [8], as a function of initial conditions. The first mechanism consisted of a series of burst-outs of the heave and pitch modes followed by partial suppression by the NES and, eventually, complete suppression. The second mechanism was partial suppression of the LCO, where the amplitude of the response was effectively reduced, but the resulting steady-state conditions were nonzero. The last mechanism resulted in complete suppression of the LCO. It was also possible to achieve no suppression. Simulations also indicated that the NES should be positioned away from the elastic axis of the wing, with aft positions giving near-optimal results; the largest basin of attraction for effective suppression.

This work was followed by a corresponding experimental study of a similar arrangement in a wind tunnel [9]. The essential nonlinearity of the NES stiffness was realized by taking advantage of the geometric nonlinearity produced when transverse displacement is induced at the center of an untensioned steel wire, clamped at both ends. In theory, this results in a purely cubic leading stiffness term, but experimentally the exponent is near 2.8. Because of hardware limitations, the NES was attached to the wing at the elastic axis and used mass ratios relative to the wing near 10% (for simulations, typical mass ratios were 1 or 2%). Nonetheless, all three LCO suppression mechanisms were observed, further validating the proposal to use TET for LCO suppression.

In continuing with the study of TET as a method to mitigate or suppress LCOs, this paper will present work that examines the effects of the attachment of an NES to an elastic-wing model. A series of ground-vibration tests were carried out on a system consisting of a uniform-thickness swept wing with a compact NES attached at the midchord of the wingtip. The design of the NES is unique to this application and will be presented in detail. In addition, a finite element (FE) model of the wing–NES system will be developed and its results compared to the experimental results. Experimental and computational data will be examined and discussed. It will be shown that localized attachment of the NES to the wing results in a strongly nonlinear system in which TET can be achieved. Furthermore, results will confirm that an NES can be designed to target a specific mode of the wing and to induce strong nonlinearity in the specific frequency range of interest. Finally, the computational model will be used to examine the conditions under which TET can occur with multiple wing modes and how the effectiveness of the NES is affected by its stiffness.

II. Nonlinear Energy-Sink Design

For this study, a compact rotary NES was designed to be attached to the tip of a model wing. Figure 2 shows detailed views of the NES components and the assembled device. The NES mass is allowed to pivot about the shaft so that the posts make contact with, and transversely deflect, the steel wires. When the device is assembled so that the undeflected steel wires experience no tension, transverse deflection results in an essentially nonlinear (nonlinearizable) stiffness.

Experimental parameter identification using several methods was performed on the NES. The restoring force surface method (RFSM) [14–17] was used to estimate the stiffness and damping of the NES. In addition, the stiffness was determined using a static test, and the damping of the bearing was estimated independently of the NES. Sensitivity of the NES parameters to the assembly procedure was examined by evaluating the stiffness and damping after three independent assemblies. In each case. the NES was assembled, tested, and then disassembled.

For each estimate of NES stiffness, the stiffness function was assumed to be

$$f_{\text{nes}}(\delta) = k_{\text{lin}}\delta + k_{\text{nl}}\text{sgn}(\delta)|\delta|^{\alpha} \tag{1}$$

where δ is the angular displacement of the NES mass. The NES damping was assumed to be viscous so that the restoring force is

$$\text{restoring force} = c_{\text{nes}}\dot{\delta} + f_{\text{nes}}(\delta) \tag{2}$$

where the overdot is used to indicate a derivative with respect to time. Figure 3a depicts a typical experimentally measured restoring torque used to identify the NES damping and stiffness parameters. Figure 3b compares the stiffness curves estimated by the static stiffness method and RFSM for the NES assembly that was used in subsequent tests. Table 1 lists the stiffness results from the RFSM tests and shows that when the coefficient of the linear term k_{lin} was assumed to be zero (i.e., when the stiffness was assumed to be essentially nonlinear), the mean squared error (MSE) was mostly unchanged. The literature suggests that an MSE of 5% or less indicates a good fit; therefore, the results show that the rotary NES design achieved a stiffness that can be approximated as essentially nonlinear. The results also showed that the stiffness in each case was nearly the same, indicating that despite the potential for variability from one assembly to another, the NES setup was repeatable.

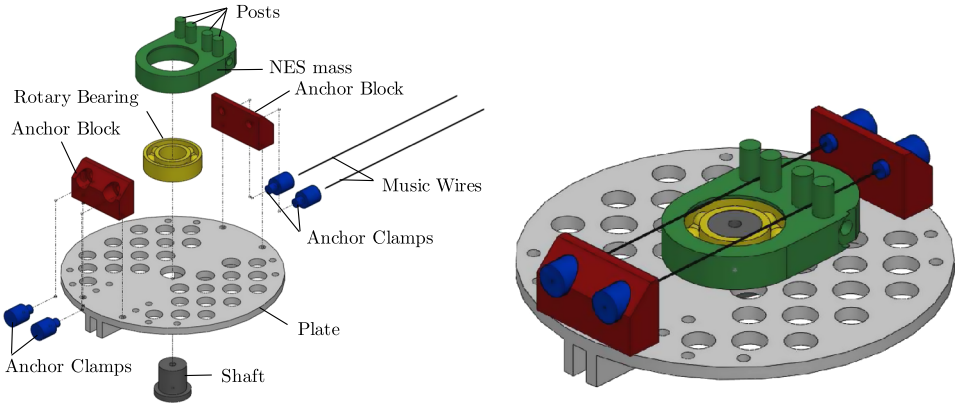

Fig. 2 Illustrations of a) exploded view of NES components and b) assembled NES.

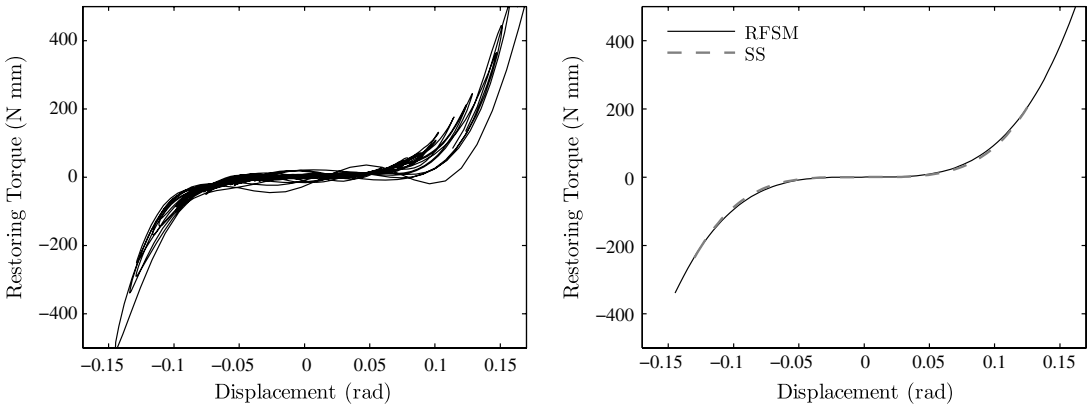

Fig. 3 Plots of a) experimentally measured restoring force for parameter identification and b) best-fit stiffness functions as determined by RFSM and static stiffness (SS) tests.

Using a viscous model, the damping of the rotary bearing was experimentally estimated to be 3.4×10^{-5} N ms/rad. However, from the RFSM tests on the fully assembled NES, the damping was estimated to be 1.07×10^{-3}, 1.10×10^{-3}, and 1.65×10^{-3} N ms/rad for cases 1, 2, and 3, respectively. The two-order-of-magnitude increase in viscous damping when the device was assembled is likely due to offaxis loading on the rotary bearing and friction between the posts and the steel wires as the NES mass rotates.

III. Uniform-Thickness Model Wing

The NES described in the preceding section was attached to the tip of a uniform-thickness, 6061-T6 aluminum alloy model wing, as shown in Fig. 4a. Details of the wing dimensions are given in Fig. 4b, which also shows the location of the clamped boundary condition that was achieved by bolting the wing between 0.25 in aluminum angle stock, which was then bolted to an optical table, as shown by Fig. 5.

In addition to the experimental model, a computational model was developed using the FE method. The wing was modeled using the four-node, 12-DOF discrete Kirchhoff quadrilateral thin-plate element [18]. For this element, the transverse displacement field is not defined in the formulation; therefore, there exists no consistent formulation for the element mass matrix. As a result, the FE model used the mass matrix formulation for the four-node Mindlin plate element using bilinear shape functions. Furthermore, a proportional damping model was adopted to construct the damping matrix of the wing based on experimental estimates of the second and sixth modal damping factors. These modal damping factors were selected because they resulted in relatively good agreement between the experimental and simulated damping factors over the first six modes. The FE code was developed and tested in MATLAB® and in FORTRAN using LAPACK libraries. All of the FE analyses were performed using the 8×32 element mesh shown in Fig. 6, with a total of 297 nodes and 891 DOF, of which 291 nodes and 873 DOF were unrestrained.

Experimental modal analysis was performed on the wing to identify its dynamics without the NES and to verify that the FE model accurately captures those dynamics in the frequency range of interest. Furthermore, modal analysis was repeated with the NES attached to the wingtip, but locked to prevent the NES mass from rotating. This did not introduce any nonlinearity to the system, but merely added a localized mass and mass moment of inertia to the wingtip; in addition, the locked attachment resulted in a chordwise stiffening of the wingtip. These effects were also considered in the corresponding FE analyses.

Experimental data acquisition was performed using a Polytec OFV 056 scanning-head laser vibrometer. Excitation was provided by a long-stroke shaker (APS Dynamics, Inc., model 400) that was driven by a single-period sine wave generated by the Smart Office software (M+P International). With this arrangement, the shaker provided an impact near the midchord of the wing, approximately 0.13 m from the root. The predicted and observed natural frequencies are listed in Table 2. Predicted and observed mode shapes of the bare wing are shown in Fig. 7, and shapes of the wing with the locked NES are shown in Fig. 8.

After developing an effective linear FE model of the wing–NES system with the NES locked (i.e., without nonlinear effects), the model was modified to include the nonlinearities of the free-to-oscillate NES. When the NES is attached to the tip of the plate wing, the motion of the NES mass is coupled to the translation and two rotational degrees of freedom of the wingtip. In modeling this configuration, the rotation about the wingtip chord was assumed to be small so that its coupling with the motion of the NES mass can be neglected. It was also assumed that the translation of the wingtip remained normal to the undeformed wing surface. The resulting arrangement can be represented by the two-dimensional schematic shown in Fig. 9.

The schematic shows the NES mounted on a massless rigid base that allows it to translate in one direction and pivot about its center. The base is attached to ground by a spring with stiffness k_{bu} and a dashpot with damping coefficient c_{bu}. The rotary motion of the entire NES assembly is coupled to the base by a spring and dashpot with stiffness and damping coefficients of $k_{b\phi}$ and $c_{b\phi}$, respectively. The translation and rotation of the NES base is represented by u and ϕ_b, respectively, while the mass and mass moment of inertia are m_b and I_b, respectively. The absolute rotation of the NES mass is denoted by ϕ_{nes} and is coupled to the NES plate by the dashpot c_{nes} and the nonlinear stiffness $f_{\text{nes}}(\delta)$, where $\delta = \phi_{\text{nes}} - \phi_b$ is the relative angle of rotation of the NES mass with respect to the NES base. Finally, m_{nes} and I_{nes} are the mass and mass moment of inertia of the NES mass, respectively, and $\bar{x}'$ is the distance from the NES center of mass to the pivot point. With that, the equations of motion (EOM) of the rotary NES mounted on a translatable base are expressed approximately as

Table 1 RFSM estimated stiffness parameters

Case	k_{lin}, N mm/rad	k_{nl}, N m/rad$^\alpha$	α	MSE
	$f_{\text{nes}}(\delta) = k_{\text{nl}}\text{sgn}(\delta)\lvert\delta\rvert^\alpha$			
1	——	77	2.75	2.32%
2	——	58	2.67	3.93%
3	——	260	3.43	4.17%
	$f_{\text{nes}}(\delta) = k_{\text{lin}}\delta + k_{\text{nl}}\text{sgn}(\delta)\lvert\delta\rvert^\alpha$			
1	153	237	3.28	1.94%
2	130	184	3.21	3.52%
3	75	354	3.61	4.06%

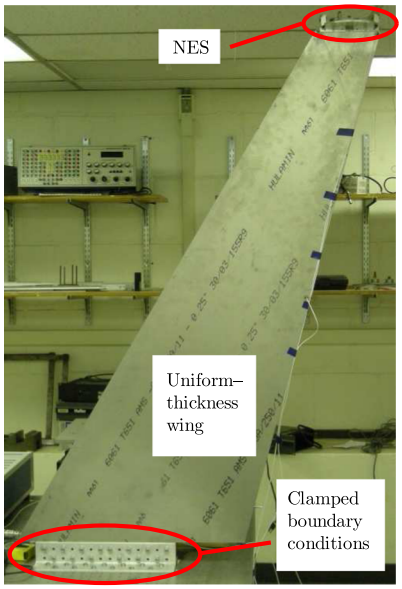

a)

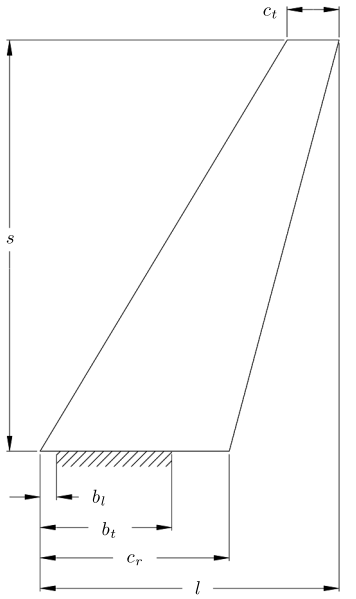

$l = 98$ cm $c_r = 62$ cm $b_t = 43.2$ cm
$b_l = 5.4$ cm $s = 135$ cm $c_t = 17$ cm

b)

Fig. 4 Geometry of the uniform-thickness plate wing: a) photograph of the experimental wing and setup and b) dimensions and boundary conditions.

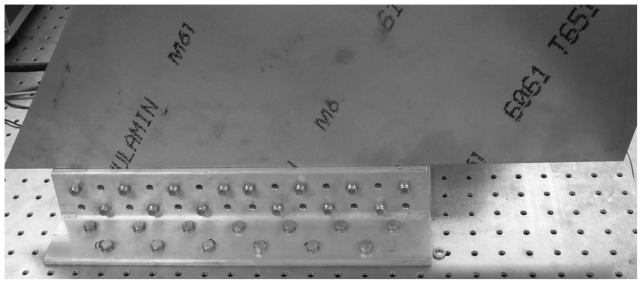

Fig. 5 Photograph of the experimental wing boundary conditions.

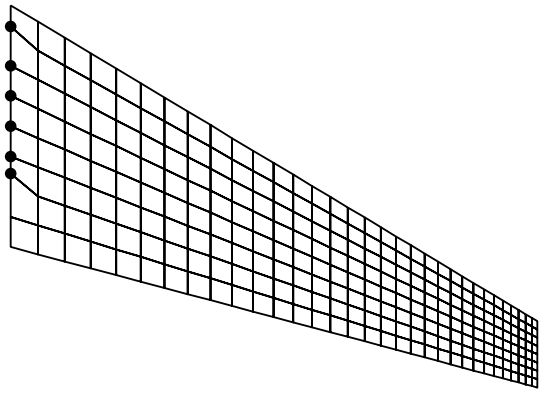

Fig. 6 8 × 32 element mesh used in FE analysis of the wing; emphasized nodes were fixed.

$$\begin{bmatrix} m_b + m_{\text{nes}} & 0 & 0 \\ 0 & I_b & 0 \\ 0 & 0 & I_{\text{nes}} \end{bmatrix} \begin{Bmatrix} \ddot{u} \\ \ddot{\phi}_b \\ \ddot{\phi}_{\text{nes}} \end{Bmatrix} + \begin{bmatrix} c_{bu} & 0 & 0 \\ 0 & c_{b\phi} + c_{\text{nes}} & -c_{\text{nes}} \\ 0 & -c_{\text{nes}} & c_{\text{nes}} \end{bmatrix} \begin{Bmatrix} \dot{u} \\ \dot{\phi}_b \\ \dot{\phi}_{\text{nes}} \end{Bmatrix} + \begin{bmatrix} k_{bu} & 0 & 0 \\ 0 & k_{b\phi} & 0 \\ 0 & 0 & 0 \end{bmatrix} \begin{Bmatrix} u \\ \phi_b \\ \phi_{\text{nes}} \end{Bmatrix} + \begin{Bmatrix} m_{\text{nes}} \bar{x}' (\ddot{\phi}_{\text{nes}} \cos\phi_{\text{nes}} - \dot{\phi}_{\text{nes}}^2 \sin\phi_{\text{nes}}) \\ f_{\text{nes}}(\phi_b - \phi_{\text{nes}}) \\ m_{\text{nes}} \bar{x}' \ddot{u} \cos\phi_{\text{nes}} + f_{\text{nes}}(\phi_{\text{nes}} - \phi_b) \end{Bmatrix} = \begin{Bmatrix} p_u(t) \\ p_{\phi b}(t) \\ p_{\phi \text{nes}}(t) \end{Bmatrix} \tag{3a}$$

or

$$\mathbf{m}\,\ddot{\mathbf{w}} + \mathbf{c}\dot{\mathbf{w}} + \mathbf{k}\mathbf{w} + \mathbf{f}^{\mathbf{nl}}(\ddot{\mathbf{w}}, \dot{\mathbf{w}}, \mathbf{w}) = \mathbf{p}(t) \tag{3b}$$

By considering the translatable base in Eq. (3) to be the wingtip of the FE model wing, the FE model was augmented so that the dynamics of the free-to-oscillate NES was included. Thus, the augmented EOM of the wing–NES system become

$$\mathbf{M}\,\ddot{\mathbf{d}} + \mathbf{C}\dot{\mathbf{d}} + \mathbf{K}\mathbf{d} + \mathbf{F}^{\mathbf{nl}} = \mathbf{P}(t) \tag{4}$$

Table 2 Predicted and observed natural frequencies (Hz) of the bare wing (no wingtip attachments) and of the wing with the NES attached and locked (added mass and chordwise stiffness)

Mode[a]	FE	Exp.	% error
		Bare wing	
1 (1B)	3.37	3.25	3.6
2 (2B)	16.73	16.41	2.0
3 (1T)	27.46	27.70	−0.9
4 (3B)	43.76	43.12	1.5
5 (2T)	67.33	68.00	−1.0
6 (4B)	83.99	82.66	1.6
7 (3T)	115.44	115.87	−0.4
		Wing with locked NES	
1 (1B)	2.75	2.66	3.5
2 (2B)	13.94	13.59	2.6
3 (1T)	27.16	27.34	−0.7
4 (3B)	37.67	36.88	2.1
5 (2T)	65.57	64.84	1.1
6 (4B)	74.15	72.81	1.8
7 (3T)	110.82	107.34	3.2

[a]B denotes out-of-plane bending, and T denotes torsion.

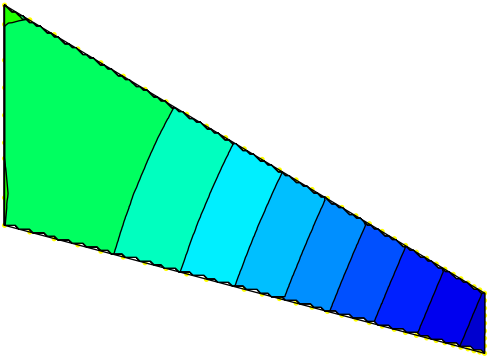

a) Mode 1 - 3.37 Hz

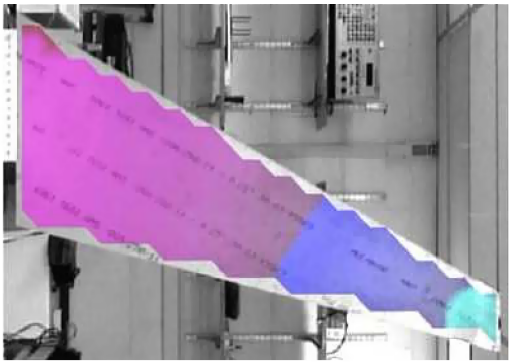

b) Mode 1 - 3.25 Hz

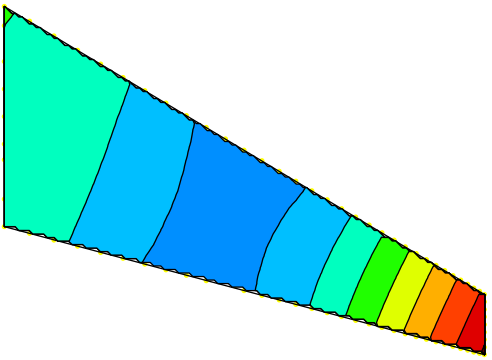

c) Mode 2 - 16.73 Hz

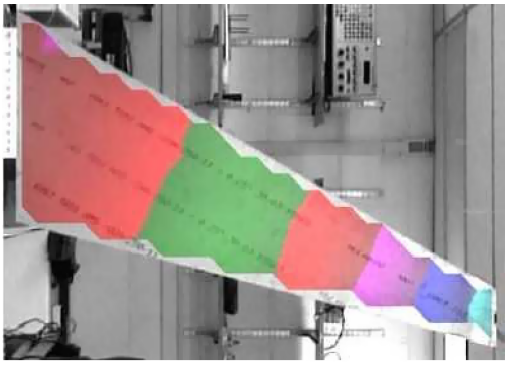

d) Mode 2 - 16.41 Hz

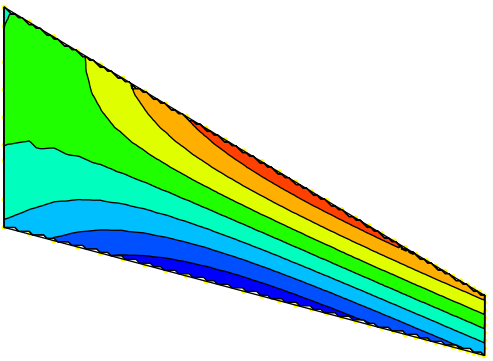

e) Mode 3 - 27.46 Hz

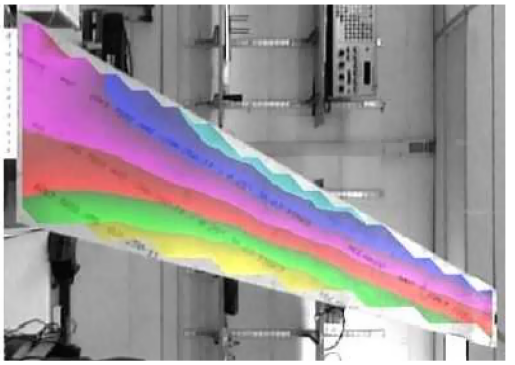

f) Mode 3 - 27.70 Hz

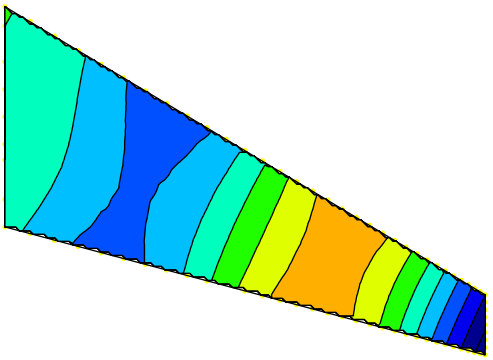

g) Mode 4 - 43.76 Hz

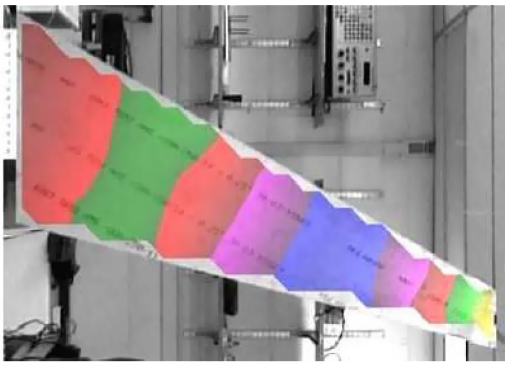

h) Mode 4 - 43.12 Hz

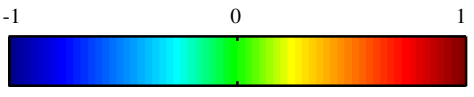

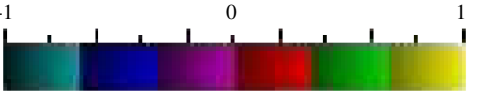

Fig. 7 Mode shapes of the bare wing: predicted (left) and experimental (right).

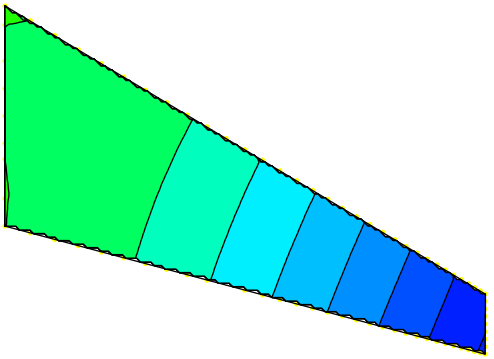

a) Mode 1 - 3.37 Hz

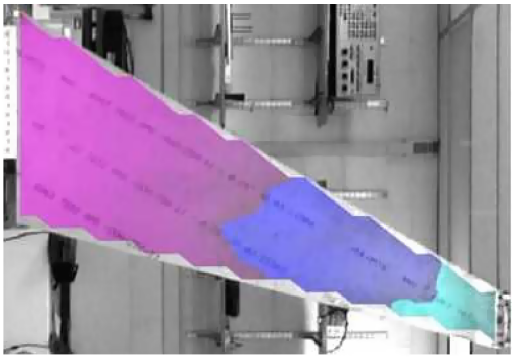

b) Mode 1 - 3.25 Hz

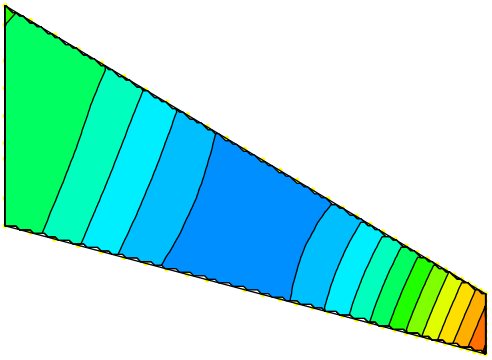

c) Mode 2 - 16.73 Hz

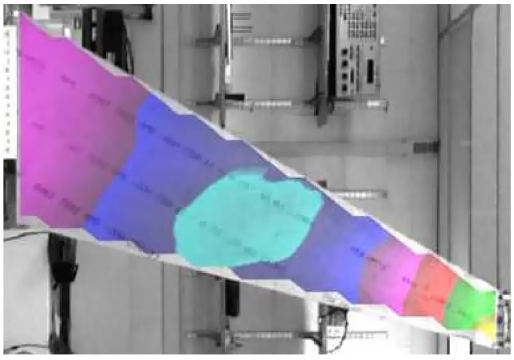

d) Mode 2 - 16.41 Hz

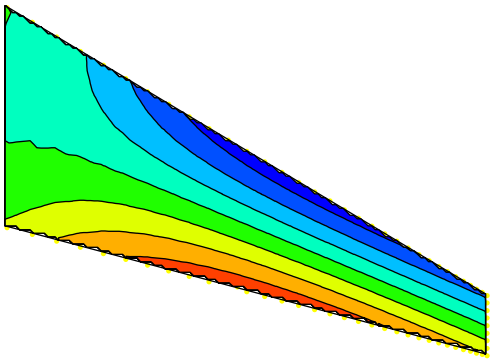

e) Mode 3 - 27.46 Hz

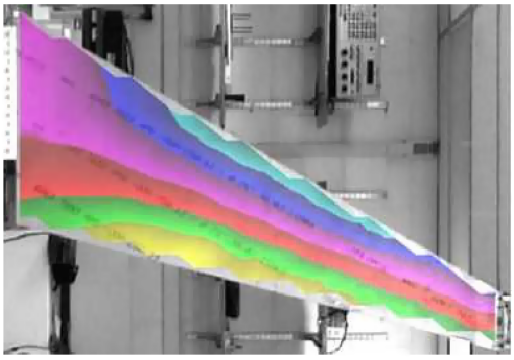

f) Mode 3 - 27.70 Hz

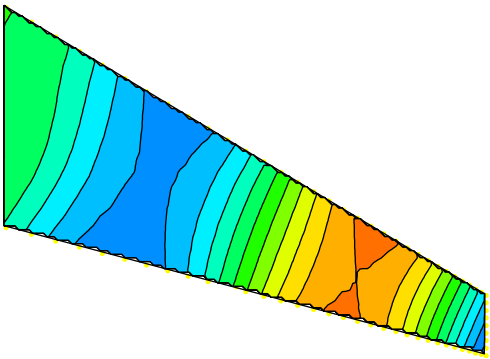

g) Mode 4 - 43.76 Hz

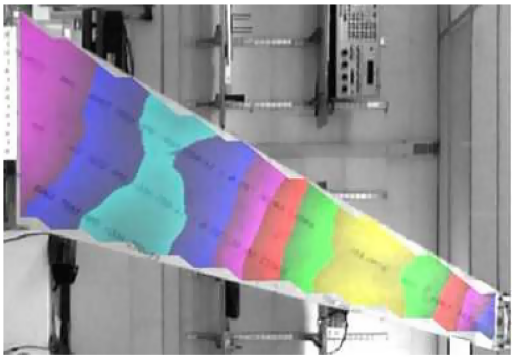

h) Mode 4 - 43.12 Hz

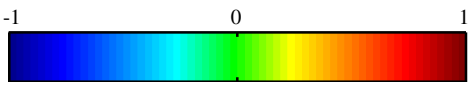

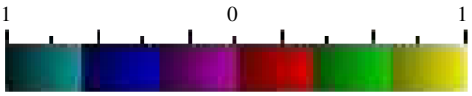

Fig. 8 Mode shapes of the wing with locked NES attached: predicted (left) and experimental (right).

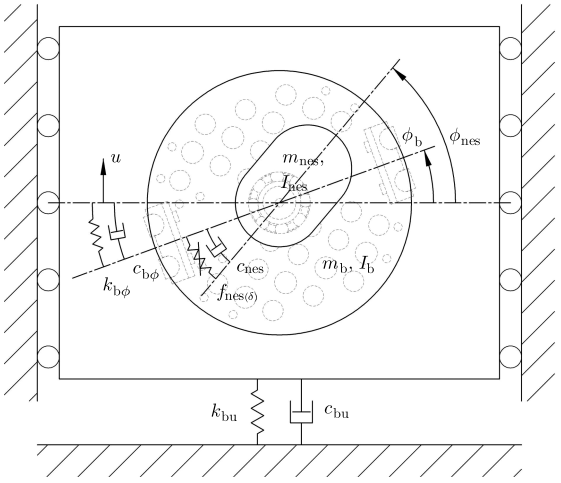

Fig. 9 Schematic of the rotary NES mounted on a base with one translation degree of freedom u and one rotational degree of freedom ϕ_b.

where **d** is a vector of the nodal DOF in the FE model with the addition of the rotation of the NES mass $\phi_{\rm nes}$, and the vector $\mathbf{F}^{\rm nl}$ contains all of the nonlinear terms. The matrices **M**, **C**, and **K** are the mass, damping, and stiffness of the augmented system and represent the linear part of the system. Furthermore, the time integrations of the nonlinear EOM were carried out using the Crank–Nicolson scheme used by Beran et al. [19].

IV. Experimental Results

With the NES free to oscillate, a series of experiments was performed. In each case, the wing was excited by an impact provided with a PCB Piezotronics impact hammer (model 086C01). The acceleration was measured at the trailing edge of the wingtip. The entire data acquisition was performed using VibPilot hardware (M+P International) and Smart Office software.

The first series of tests attempted to identify the frequencies over which the wing, with the NES attached (the configuration shown in Fig. 4a), exhibits a strongly nonlinear response when subjected to a hammer impact and how much energy is required to realize this strongly nonlinear response. This was accomplished, first, by evaluating the experimental accelerance frequency response function (FRF) for response and excitation measured at the locations shown in Fig. 10, with the NES attached to the wing, but locked to prevent oscillation of the mass; thus, the essentially nonlinear stiffness was not yet introduced into the system, so that it can still be considered linear. Next, an identical test was performed to experimentally measure the FRF from a single time series, but with the NES free to oscillate, thus introducing the potential for strongly nonlinear response. With the NES free to oscillate, this was repeated several times for increasing excitation magnitudes. In each test, data were sampled at 1024 Hz for approximately 8 s.

It is important to mention that for a nonlinear system, no FRF can be defined in a classical sense, because the response of the system to a periodic excitation is strongly dependent on the magnitude of the excitation and might possess strong harmonic components different than the excitation frequency. Hence, only the magnitude of the harmonic of the response at the frequency of the excitation was taken into account when defining the nonlinear FRF. Nonetheless, the FRF of the nonlinear system can be used to gain some understanding of the circumstances under which the response of the system diverges from the linear approximation; an alternative frequency decomposition of the nonlinear time series, using wavelet transforms, will be discussed later. In this case, it is expected that for lower magnitudes of excitation, the experimental accelerance FRF of the free-to-oscillate system will remain virtually unchanged from the FRF of the system with the NES locked, since the nonlinear effects induced by the NES are not profound at these lower energy regimes. However, at higher energy regimes provided by forceful hammer impacts, the response of the system will become strongly nonlinear, the measured nonlinear FRF will show a clear departure from the FRF of the linear system, and the nonlinear effects induced by the NES will become apparent. It will be of particular interest to study the frequency ranges where the nonlinear effects are more profound, since this will demonstrate the efficacy of the NES to induce nonlinearity and strongly affect specific modes of the wing.

The magnitudes of the experimental FRFs are shown in Fig. 11. The results show that when the NES was free to oscillate and the wing–NES system was excited by a relatively weak pulse with peak magnitude of approximately 480 N, the magnitude of the measured FRF was nearly identical to that measured for the system with the NES locked. This indicates that at such a low excitation level, the system could be approximated by a linear model for the range of frequencies examined here. However, this was no longer true when the system experienced an excitation with a relatively strong peak magnitude of approximately 800 N. Under those circumstances, the magnitude of the experimental accelerance FRF significantly departed from that of the system, with the NES locked in the frequency ranges of 5–25 and 40–70 Hz, indicating that the response was strongly nonlinear in these ranges. What is even more significant is that the frequency of the linearized second bending mode (13.6 Hz) fell within the first range of strongly nonlinear response, resulting in a reduction of its peak magnitude of nearly 70% relative to the FRF of the linear system. Furthermore, new peaks in the magnitude of the FRF appear in the vicinity of 20 Hz; it is likely that this is a manifestation of excitation of strongly nonlinear modes, as discussed below. This combination of features is indicative of targeted energy transfer from the second bending mode of the wing to the NES; this will be discussed in greater detail in what is to follow.

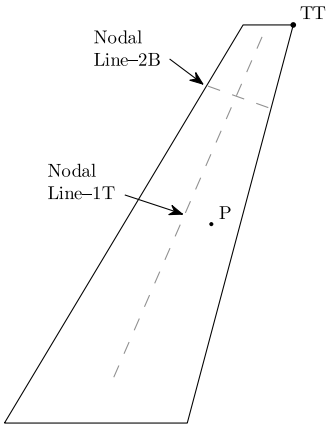

Fig. 10 Locations of the pulse excitation, P, and the response at the trailing tip of the wing, TT, for experimental accelerance FRFs with the NES locked and with the NES free to oscillate.

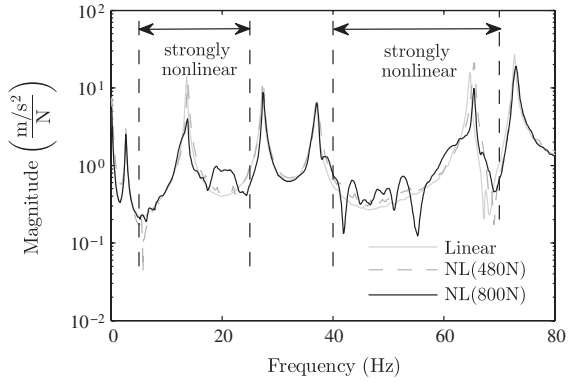

Fig. 11 Experimental accelerance FRF (excitation and response locations are given in Fig. 10) evaluated from a single time series (no averaging) for two excitation magnitudes for the wing–NES system with the NES free to oscillate and for the wing–NES system with the NES locked to prevent oscillation (linear system).

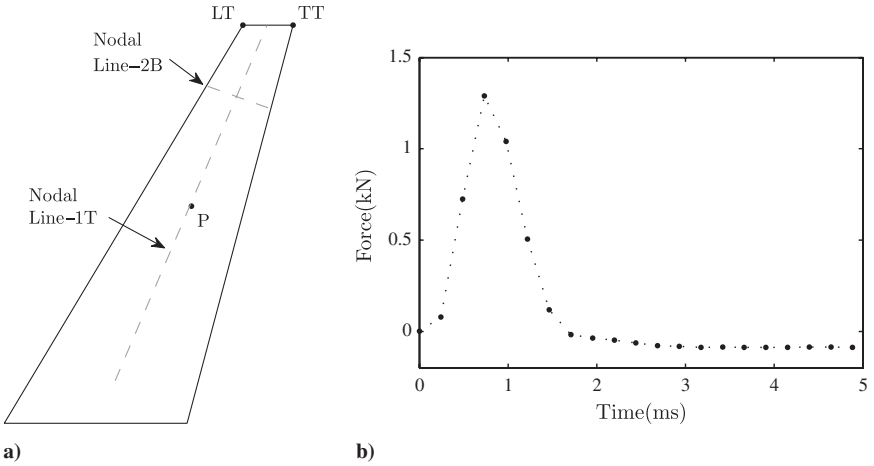

Fig. 12 Illustrations of a) locations of the hammer impact (P) and the measured response (TT) and b) experimentally measured force pulse.

Although the previous results are valuable, FRFs of nonlinear systems are limited in the information that they can convey. To better understand the strongly nonlinear dynamics that took place, one must examine the evolution of the response in the frequency–time domain. To do that, let us examine a second experimental example in which the wing NES, with the NES free to oscillate, was excited by a hammer impact near the antinode of the second bending mode and the nodal lines of the first torsional and third bending modes, as indicated by Fig. 12a. The measured force of the impact is given in Fig. 12b, and the consequent response of the wing was measured by a PCB Piezotronics accelerometer at the trailing edge of the wingtip. Data were sampled at 4096 Hz for approximately 8 s using the M+P International VibPilot system. The velocity response of the wingtip trailing edge was estimated by numerical integration of the measured acceleration using the trapezoidal rule. Furthermore, the Morlet wavelet transform (WT) was applied to the velocity response to decompose the frequency components as a function of time. The WT is similar to the Fourier transform in that it transforms a response in the time domain to the frequency domain; however, it does this over small segments of time, rather than the entire response, allowing one to see which frequency components dominate the response over each time segment. This is especially useful for studying damped nonlinear dynamics, because the frequencies of the harmonics are related to the energy in the system and therefore change as energy is dissipated.

Figure 13 shows the WT of the experimental nonlinear response of the wing–NES system (with the NES free to oscillate). Since the excitation was provided near the intersection of the nodal lines of the first two torsional modes with the third bending mode, the response was nearly limited to the first two bending modes, plus some minor participation of the fourth bending mode at a frequency of around 75 Hz. The WT indicates the relative intensity of the frequency components of the response and shows that the response was initially dominated by the first two bending modes. However, closer inspection suggests a brief resonance capture at approximately 18.1 Hz that lasted about 0.25 s. This does not correspond to any of the linearized natural frequencies of the wing–NES system; instead, it is consistent with 4:3 resonance capture of a nonlinear mode. Furthermore, the intensity of the response in the second bending mode was significantly reduced within the first 0.6 s following the excitation, and it no longer appears in the WT after 1.5 s. This, combined with evidence of a 4:3 resonance capture with respect to the second bending mode, indicates that targeted energy transfer from the wing to the NES was realized. In particular, these observations suggest that a significant portion of the energy initially in the second bending mode was transferred to the NES, where it was rapidly dissipated locally. These results are critical, as they indicate the efficacy of a relatively lightweight and compact NES to passively absorb energy from a specific mode of a continuously flexible structure and dissipate it. But as shown below, the NES is capable of additional, more complex, nonlinear dynamic behavior: that is, broadband energy absorption. Indeed, the NES is capable of transiently resonating with multiple nonlinear modes of the wing, extracting energy from each before engaging in resonance with the next.

V. Computational Results

Although the experimental results are compelling, the available data were not able to explain all of the phenomena, because the response of the NES mass could not be easily or reliably measured in the experiment. However, a robust computational model can be used to provide more insight into the nonlinear dynamics. As a result, the previous example described by Fig. 12 was simulated using the FE model. The force pulse used in the simulation was interpolated from the measured force from the experimental example after it was

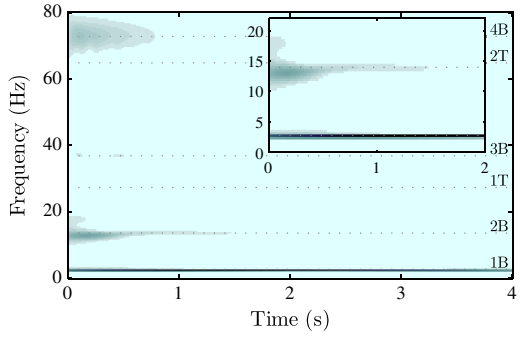

Fig. 13 Wavelet transform of the experimental velocity response at the trailing edge of the wingtip to the excitation described in Fig. 12; the inset shows a closer view, indicating 4:3 resonance capture of a nonlinear mode.

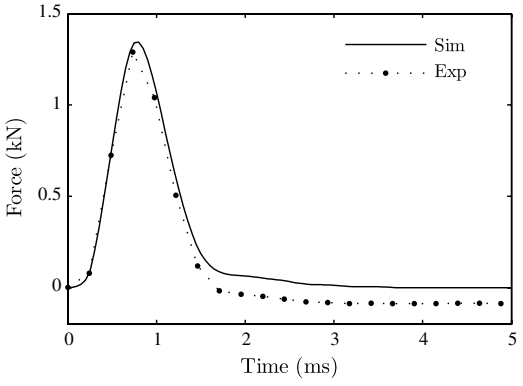

Fig. 14 Experimentally measured force pulse and the interpolated pulse used in the simulation after correcting for transducer charge leakage.

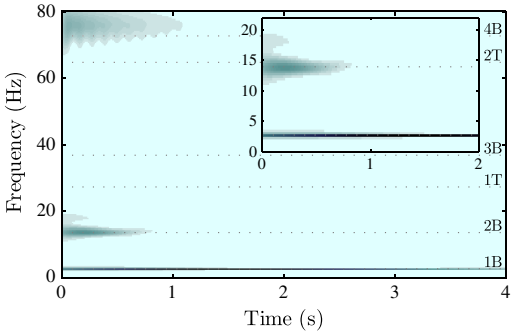

Fig. 15 Wavelet transform of the simulated velocity response at the trailing edge of the wingtip to the excitation described in Fig. 14; these results correspond to the experimental WT in Fig. 13.

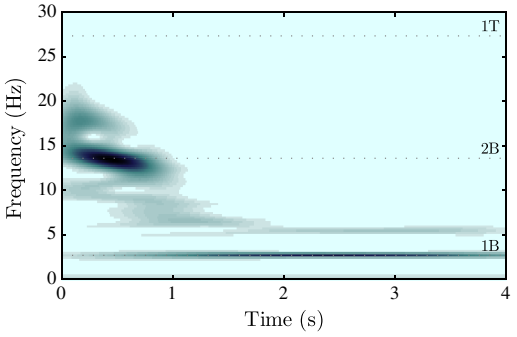

Fig. 16 Wavelet transform of the simulated relative displacement response of the NES mass (ϕ_{nes}) indicating 4:3 resonance capture and fundamental TET with respect to the second bending mode of the wing.

corrected for transducer charge leakage. A comparison of the two pulses is given in Fig. 14. The NES stiffness was estimated from the third case of Table 1 with the coefficient of the linear term k_{lin} assumed to be zero and the damping coefficient c_{nes} assigned the value of 1.65×10^{-3} N ms/rad. To accurately preserve the force profile in the simulation, a time step of 50 μs was used over its duration. At the end of the pulse, the time step was extended to 250 μs and remained constant for the remainder of the simulation. Upon completion of the simulation, the resulting data were interpolated at 4096 Hz, using the linear interpolation function in MATLAB, to match the sampling rate of the corresponding experimental data.

Similar to the experimental results, the WT of the velocity response at the trailing edge of the wingtip in Fig. 15 indicates 4:3 resonance capture of a nonlinear mode with respect to the second bending frequency. This transient phenomenon in the computational results agrees well in relative intensity and duration with the experimental measurement, suggesting that the FE model has accurately captured the strongly nonlinear dynamics of the system. Furthermore, the simulation indicated that most of the response in the second bending mode would be rapidly dissipated within about 0.7 s, in accordance with the experimental results.

With confidence in the FE model, it was useful to examine the simulated response of the NES mass to better understand the complex nonlinear dynamics of the wing–NES resonant interaction. Figure 16 shows the WT of the simulated relative angular displacement of the NES mass (ϕ_{nes}). From this, it becomes clear that the response of the NES mass was initiated by 4:3 resonance capture of a nonlinear mode, which triggered fundamental TET with respect to the second bending mode. This is indicated in the WT by the intense band appearing near the natural frequency of the second bending mode, beginning approximately 0.1 s after the system was excited and ending before 1 s into the response. It was during this time that the response of the system became localized to the NES, allowing it to become highly excited and to dissipate a significant portion of the energy in the linearized second bending mode. The frequency at which fundamental resonance capture occurred was not constant; instead, it began at a frequency slightly greater than that of the natural frequency of the second bending mode and ended slightly below, suggesting that the response was evolving along the backbone of the frequency energy plot (FEP) of the system. Upon escape from fundamental resonance capture, TET stopped, and the response transitioned to a lower energy branch of the FEP, interacting with the

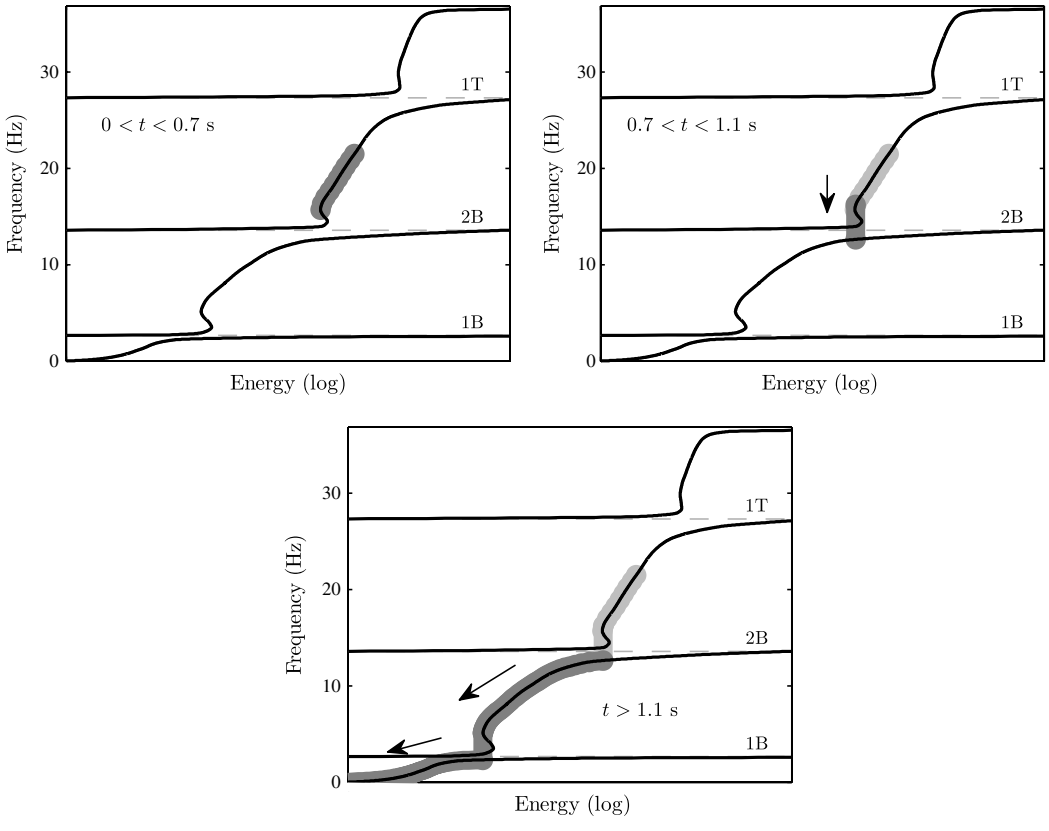

Fig. 17 Explanation of the simulated response of the wing–NES system in terms of a schematic FEP.

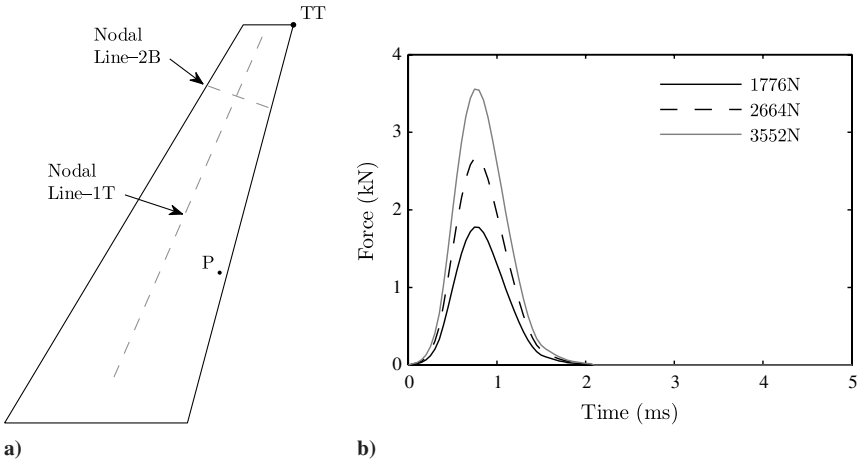

Fig. 18 Illustrations of a) locations of the simulated excitation (P) and response (TT) and b) three excitations considered.

first bending mode of the system. Figure 17 summarizes the response of the wing–NES system in terms of a schematic of its FEP.

The FEP describes the possible responses of the undamped and unforced nonlinear system, given some initial conditions and internal energy. In some ways, the FEP is the nonlinear analog to the FRF of a linear system. The backbone represents the main branch(es) of the FEP, from which secondary branches, or tongues, extend. For each frequency and energy there are numerous solutions to the system,

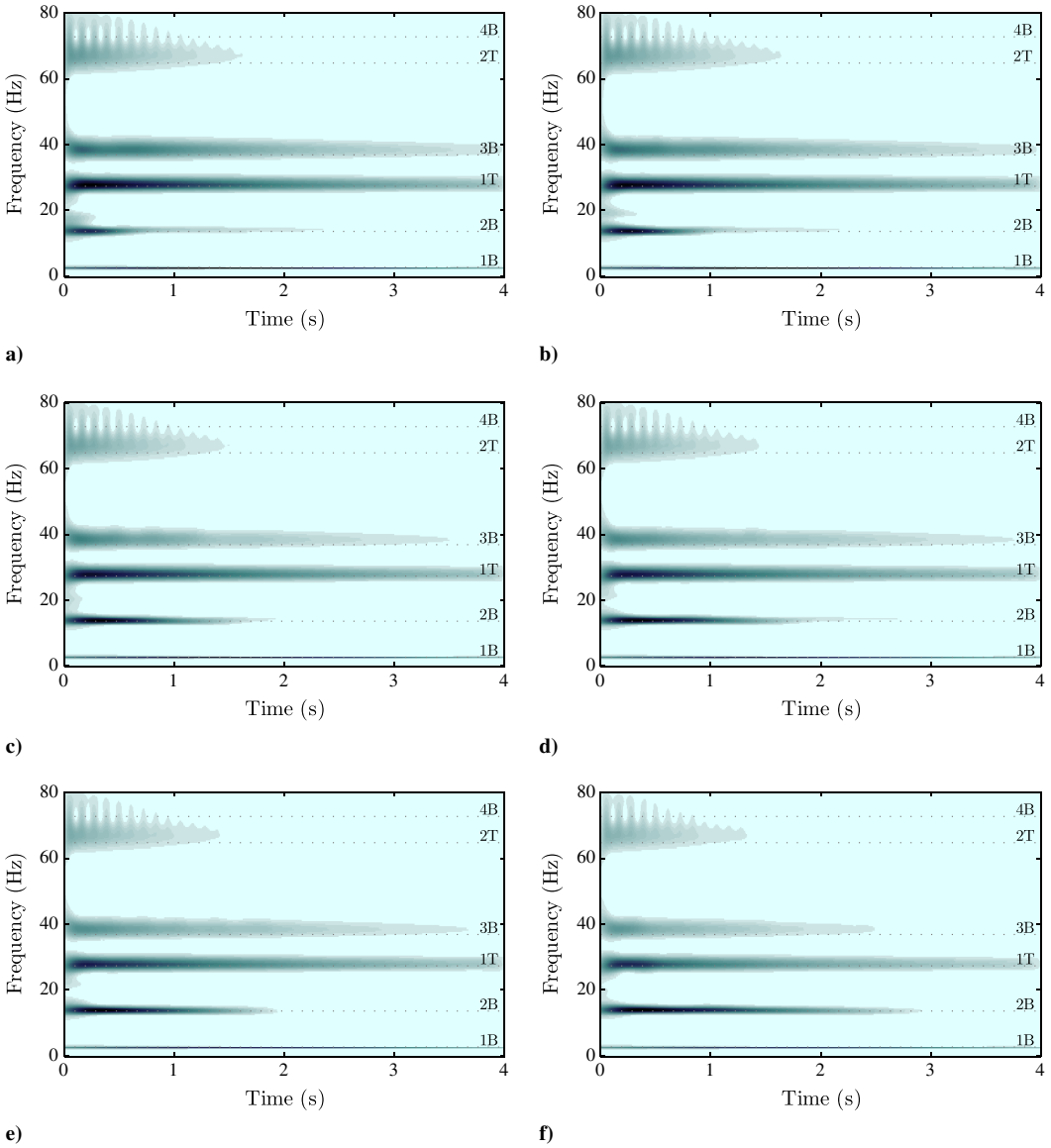

Fig. 19 Simulated WTs of the velocity time histories at the trailing tip of the wing for multiple force pulse magnitudes; the left column shows results which that considered the experimentally determined NES stiffness ($f_{\text{nes}}^{(1)}$) and on the right, an increased NES stiffness was considered ($f_{\text{nes}}^{(2)}$); 1776 N pulse (top), 2664 N pulse (middle), and 3552 N (bottom).

however, only a few are significant to TET. The FEP remains applicable to lightly damped nonlinear systems like the wing and NES. The inclusion of damping allows the free response to evolve over time as energy is dissipated; i.e., the response of the system may transition from one branch to another. For additional explanation, the reader is referred to Kerschen et al. [20] and Lee et al. [21].

These results provide further confirmation that the compact rotary NES effectively achieved TET from the elastic wing. Examples given thus far have shown that the current NES configuration absorbs energy mainly from the second bending mode of the wing; however, if the NES is to be used to mitigate LCOs that involve interaction between multiple modes, it should be able to interact with more than one of those modes. For a wing–NES system similar to the one studied here, it would be desirable for the NES to interact with the first torsional mode in addition to the second bending mode. To examine the circumstances under which TET from the first torsional mode is induced, a series of simulations was performed. These simulations examined what type of excitation would be required to achieve TET from the first torsional mode to the NES and whether a change in the NES stiffness function would have a significant effect on TET.

For this series of simulations, the excitation was applied at location P in Fig. 18a, near the antinodes of the second bending and first torsional modes. The pulse profile given in Fig. 18b was scaled to produce three similar excitations with peak-force magnitudes of 1776, 2664, and 3552 N, respectively. For each excitation, two simulations were performed; one considered the same NES stiffness function as in the previous examples, $f_{\text{nes}}^{(1)}(\delta) = (260\ \text{N m}/\text{rad}^{\alpha})\text{sgn}(\delta)|\delta|^{3.43}$, and another approximated the stiffness for wire diameter changed from 0.025 to 0.032 in., thus increasing the nonlinear coefficient k_{nl} from 260 to 430 $\text{N m}/\text{rad}^{\alpha}$. In each case, the NES damping coefficient remained constant at 1.65×10^{-3} N ms/rad.

Wavelet transforms of the response at the trailing edge of the wingtip for each combination of excitation and NES stiffness are shown in Fig. 19. The results look very similar to the previous simulated and experimental examples, with the exception, of course, that all of the first five linearized modes were excited. The response to the pulse with a peak-force magnitude of 1776 N for $f_{\text{nes}}^{(1)}$ and $f_{\text{nes}}^{(2)}$ look much the same and include resonance capture of nonlinear modes as well as apparent TET from the second bending mode. With the increase in stiffness, though, the nonlinear mode excited was at a

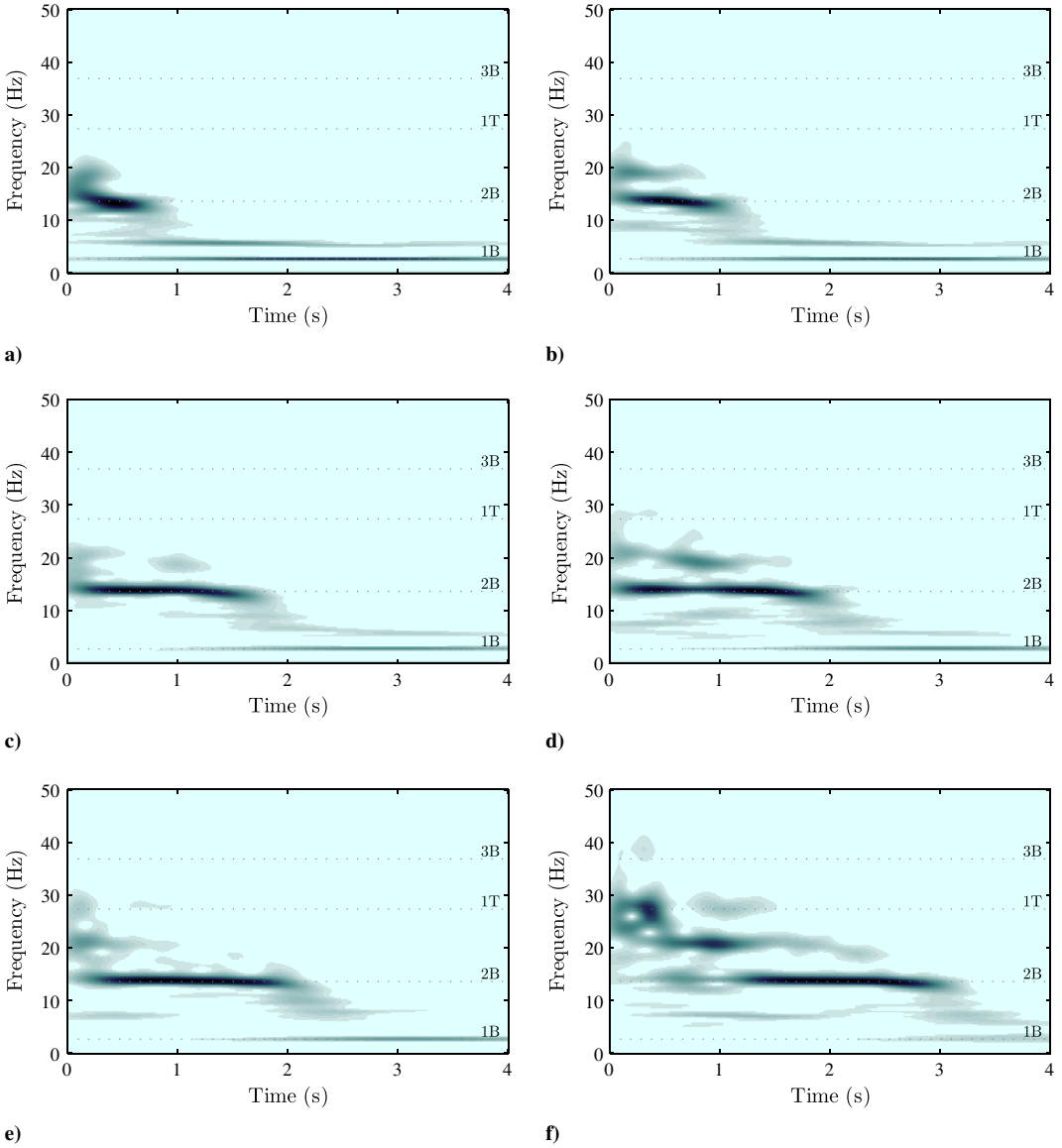

Fig. 20 Simulated WTs of the displacement time histories of the NES mass, relative to the wingtip, for multiple force pulse magnitudes; the left column shows results that considered the experimentally determined NES stiffness ($f_{\text{nes}}^{(1)}$) and on the right, an increased NES stiffness was considered ($f_{\text{nes}}^{(2)}$); 1776 N pulse (top), 2664 N pulse (middle), and 3552 N (bottom).

higher frequency, near 7:5 resonance capture, rather than 4:3 as in the previous case. This is not unexpected, because the increase in NES stiffness shifts the system's FEP lower (or to the left) on the energy scale, therefore requiring less energy to excite higher-frequency modes. Increasing the excitation to a peak-force magnitude of 2664 N provided a slight change in the response from the previous case. Resonance captures with nonlinear modes occurred at higher frequencies for both NES stiffnesses, and there is a slight reduction in the duration of the response in the third bending mode. Furthermore, the duration of intense response of the second bending mode was increased slightly for both stiffnesses, though more so for $f_{\text{nes}}^{(2)}$. This trend continued as the excitation level was increased further. In the last case it is evident that the duration of the response in the third bending mode was significantly reduced when the NES stiffness was equal to $f_{\text{nes}}^{(2)}$.

As before, the WTs of the NES response (Fig. 20) are useful in gaining a better understanding of the dynamics that took place. As was gathered from the wingtip response to the 1776 N excitation, the WTs look nearly identical to the previous example and can be similarly explained. However, when the force was increased to the next level, 2664 N, the dynamics appear to have changed. With an NES stiffness of $f_{\text{nes}}^{(1)}$, the initial response included components of strongly nonlinear modes, including a 1:1 resonance with respect to the second bending mode. Unlike the previous examples, where the frequency at which 1:1 resonance capture occurred with the second bending mode was transient, here it persisted at constant frequency over approximately 1.1 s of the 1.6 s capture. This likely indicated that the 1:1 resonance capture began at higher energy than before, allowing for fundamental TET to be sustained for a longer period of time. The same was true when the NES stiffness was $f_{\text{nes}}^{(2)}$ although, in this case, the higher-frequency nonlinear modes were a more significant portion of the response. In fact, there are some indications of a brief resonance capture even with the first torsional mode. These results clearly demonstrate the capacity of the lightweight NES to engage in transient resonance (transient resonance capture) with multiple wing modes, in a phenomenon termed resonance capture cascade [12].

The response of the system to the highest level of excitation, corresponding to a peak force of 3552 N, demonstrated exceptionally complex dynamics. Beginning with NES stiffness $f_{\text{nes}}^{(1)}$, the response of the NES mass was dominated by transient resonance capture at the second bending frequency of the linearized system. Like before, this resulted in TET from the wing to the NES; however, in the first second of the response, several nonlinear modes appeared to be engaged in transient resonance, including the first torsional mode. While this showed interaction with the torsional mode, it did not necessarily indicate TET. In fact, from the WT of the wingtip in this case (Fig. 19e) it seems unlikely that a significant portion of the energy in the first torsional mode was dissipated by TET to the NES.

When the NES stiffness was increased to $f_{\text{nes}}^{(2)}$, the first 0.5 s of the NES response occurred predominantly near the frequency of the first torsional mode. This was concluded by an abrupt transition to a lower-frequency mode and the subsequent realization of TET with the second bending mode of the wing. This is ab excellent example of a resonance capture cascade that includes TET from two modes of the wing (first torsional and second bending) as well as numerous transient resonance captures with nonlinear modes. In addition, there is some evidence of brief resonance interaction with the third bending mode of the wing. This is indicated in Fig. 20f by the shaded region near the third bending frequency at about 0.3 s and supported by the significant reduction in the duration of the wingtip response in that mode (Fig. 19f). Figure 21 summarizes the response of the wing–NES system to the 3552 N excitation.

The results of this series of simulations show that it is possible for the wing, with the NES attached in its current configuration, to interact with modes higher than second bending. This also suggests that using a stiffer NES can reduce the amount of energy required to initiate resonance with higher-frequency modes. The ability to induce interaction between torsional modes of the wing and the NES, while the NES pivots about an axis located at the midchord of the

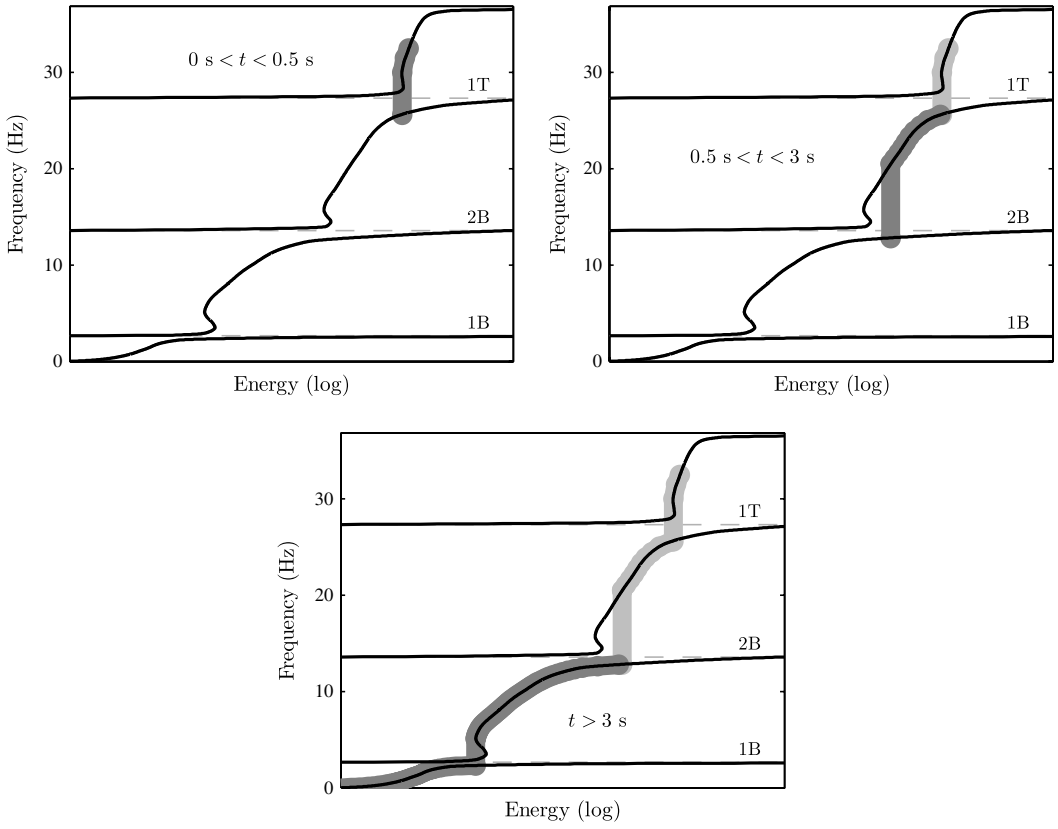

Fig. 21 Explanation of the simulated response of the nonlinear system with stiffness $f_{\text{nes}}^{(2)}$ to a force pulse with a peak magnitude of 3552 N, in terms of a schematic FEP.

wingtip, is encouraging because this is the least desirable position for the NES to interact with the lowest torsional modes. Judging from term $\mathbf{f}^{\mathbf{nl}}$ in Eq. (3), it is clear that the NES is extremely sensitive to acceleration normal to the wing at the midchord of the wingtip, $\ddot{u}$. However, the nodal lines of the low-frequency torsional modes intersect the axis of rotation of the NES, resulting in zero transverse acceleration, leaving only the less effective, direct coupling between the NES stiffness and wingtip rotations. From this, it seems likely that significant improvements in the effectiveness of the NES may be realized by optimizing its chordwise position at the wingtip.

VI. Conclusions

A compact rotary nonlinear energy sink was developed to study targeted energy transfer applications related to aeroelasticity. It was shown experimentally that the NES could be constructed to possess a stiffness in the form of a nearly pure power function with typical exponents slightly greater than three. This essentially nonlinear, or nonlinearizable, stiffness is a critical characteristic of the NES, since it allows it to resonate with any arbitrary set of modes of the structure to which it is attached. That is, the NES does not possess a preferential resonance frequency, and its instantaneous frequency of oscillation is time-varying, depending on its instantaneous energy.

With the NES attached to a uniform-thickness swept wing, a series of tests was performed in which the wing was excited by hammer impacts of varying magnitude at several locations. Behavior clearly indicating a minimum energy threshold beyond which TET occurs was observed in experiments and simulations. Furthermore, when enough energy was imparted to the system, strongly nonlinear resonance interactions between the NES and the second bending mode were recorded. Simulated responses corresponding to these experiments confirmed the presence of TET, which dissipated energy in the second bending mode of the wing, dramatically reducing the amplitude of the response in that mode. In addition, a series of simulations was performed to consider the effects of increased NES stiffness and to observe TET from the first torsional mode of the wing. The results showed that even though the NES was attached to the wing at or near the nodal line of the first torsional mode, its rotary motion allowed for some nonlinear interactions. In particular, for increased NES stiffness and a large-enough excitation, 1:1 resonance capture was observed with the first torsional mode.

It can be concluded from this study that TET is attainable for transient or broadband excitations by attaching the compact NES to the tip of a model wing. Experimental and simulated results clearly showed such complex nonlinear phenomena as nonlinear beating, resonance captures, and resonance capture cascades. Furthermore, simulations suggest that it is possible to modify the design of the NES to make it interact with the first torsional and other higher modes, in addition to the second bending mode.

The computational and experimental results reported in this work are important from the LCO suppression point of view, since they demonstrate that the NES at the tip of the model wing can induce strongly nonlinear effects and drastically reduce the response of selected wing modes responsible for LCO triggering and development. Moreover, it can perform this through complex resonance capture cascades over broad frequency ranges. Because of its essential stiffness nonlinearity, the local NES can induce global changes in the dynamics of the wing, as it can resonantly interact with, and affect, wing modes over broad frequency and energy ranges. This result will be important in future work when the NES will be applied to suppress aeroelastic instability in a practical inflow wing system.

Acknowledgments

The authors wish to acknowledge the financial support of this effort by the U.S. Air Force Office of Scientific Research (AFOSR) through the following Small Business Technology Transfer contracts: Phase I: "Physics-Based Identification and Management of Aeroelastic Limit-Cycle Oscillations (LCO)-Phase I," prime contract number FA9550-07-C-0070. Phase II: "Physics-Based Identification and Management of Aeroelastic Limit-Cycle Oscillations (LCO)-Phase 2," prime contract number FA9550-09-C-0057. Victor Giurgiutiu and David Stargel were the AFOSR Program Directors during the course of this work. The prime contractor for both phases of the STTR was NextGen Aeronautics, Inc., of Torrance, California.

References

[1] Block, J. J., and Strganac, T. W., "Applied Active Control for a Nonlinear Aeroelastic Structure," *Journal of Guidance, Control, and Dynamics*, Vol. 21, No. 6, 1998, pp. 838–845. doi:10.2514/2.4346

[2] Ko, J., Strganac, T. W., and Kurdila, A. J., "Adaptive Linearization for the Control of a Typical Wing Section with Torsional Nonlinearity," *Nonlinear Dynamics*, Vol. 18, 1999, pp. 289–301. doi:10.1023/A:1008323629064

[3] Platanitis, G., and Strganac, T. W., "Control of a Nonlinear Wing Section Using Leading- and Trailing-Edge Surfaces," *Journal of Guidance, Control, and Dynamics*, Vol. 27, No. 1, 2004, pp. 52–58. doi:10.2514/1.9284

[4] Lee, Y. S., Vakakis, A. F., Bergman, L. A., McFarland, D. M., Kerschen, G., Nucera, F., Tsakirtzis, S., and Panagopoulos, P. N., "Passive Nonlinear Targeted Energy Transfer and Its Applications to Vibration Absorption: A Review," *Proceedings of the Institution of Mechanical Engineers, Part K (Journal of Multi-Body Dynamics)*, Vol. 222, No. 2, 2008, pp. 77–134. doi:10.1243/14644193JMBD118

[5] McFarland, D. M., Bergman, L. A., and Vakakis, A. F., "Experimental Study of Nonlinear Energy Pumping Occurring at a Single Fast Frequency," *International Journal of Non-Linear Mechanics*, Vol. 40, 2005, pp. 891–899. doi:10.1016/j.ijnonlinmec.2004.11.001

[6] Gendelman, O., Manevitch, L. I., Vakakis, A. F., and M'Closkey, R., "Energy Pumping in Nonlinear Mechanical Oscillators: Part I. Dynamics of the Underlying Hamiltonian Systems," *Journal of Applied Mechanics*, Vol. 68, 2001, pp. 34–41. doi:10.1115/1.1345524

[7] Vakakis, A. F., and Gendelman, O., "Energy Pumping in Nonlinear Mechanical Oscillators: Part II. Resonance Capture," *Journal of Applied Mechanics*, Vol. 68, 2001, pp. 42–48. doi:10.1115/1.1345525

[8] Lee, Y. S., Vakakis, A. F., Bergman, L. A., McFarland, D. M., and Kerschen, G., "Suppressing Aeroelastic Instability Using Broadband Passive Targeted Energy Transfer, Part 1: Theory," *AIAA Journal*, Vol. 45, No. 3, 2007, pp. 693–711. doi:10.2514/1.24062

[9] Lee, Y. S., Kerschen, G., Vakakis, A. F., Bergman, L. A., and McFarland, D. M., "Suppressing Aeroelastic Instability Using Broadband Passive Targeted Energy Transfer, Part 1: Theory," *AIAA Journal*, Vol. 45, No. 10, 2007, pp. 2391–2400. doi:10.2514/1.28300

[10] McFarland, D. M., Beran, P. S., Lee, Y. S., Bergman, L. A., and Vakakis, A. F., "Transonic aeroelastic analysis including the effects of a nonlinear energy sink," *Collection of Technical Papers-AIAA/ASME/ASCE/AHS/ASC Structures, Structural Dynamics and Materials Conference*, Vol. 4, AIAA, Reston, VA, 2007, pp. 3898–3905.

[11] Lee, Y. S., Vakakis, A. F., Bergman, L. A., McFarland, D. M., and Kerschen, G., "Enhancing the Robustness of Aeroelastic Instability Suppression Using Multi-Degree-Of-Freedom Nonlinear Energy Sinks," *AIAA Journal*, Vol. 46, No. 6, 2008, pp. 1371–1394. doi:10.2514/1.30302

[12] Vakakis, A. F., Gendelman, O. V., Bergman, L. A., McFarland, D. M., Kerschen, G., and Lee, Y. S., *Nonlinear Targeted Energy Transfer in Mechanical and Structural Systems*, Springer, New York, 2008.

[13] Lee, Y. S., Vakakis, A. F., Bergman, L. A., McFarland, D. M., and Kerschen, G., "Triggering Mechanisms of Limit Cycle Oscillations Due to Aeroelastic Instability," *Journal of Fluids and Structures*, Vol. 21, 2005, pp. 485–529. doi:10.1016/j.jfluidstructs.2005.08.011

[14] Kerschen, G., Lenaerts, V., Marchesiello, S., and Fasana, A., "A Frequency Versus a Time Domain Identification Technique for Nonlinear Parameters Applied to Wire Rope Isolators," *Journal of Dynamic Systems, Measurement, and Control*, Vol. 123, 2001, pp. 645–650. doi:10.1115/1.1410368

[15] Kerschen, G., and Golinval, J. C., "Theoretical and Experimental Identification of a Nonlinear Beam," *Journal of Sound and Vibration*, Vol. 244, No. 4, 2001, pp. 597–613. doi:10.1006/jsvi.2000.3490

[16] Kerschen, G., Lenaerts, V., and Golinval, J. C., "VTT Benchmark: Application of the Restoring Force Surface Method," *Mechanical Systems and Signal Processing*, Vol. 17, No. 1, 2003, pp. 189–193. doi:10.1006/mssp.2002.1558

[17] Masri, S. F., and Caughey, T. K., "Nonparametric Identification Technique for Nonlinear Dynamic Problems," *Journal of Applied Mechanics*, Vol. 46, No. 2, 1979, pp. 433–447.

[18] Batoz, J., and Tahar, M. B., "Evaluation of a New Quadrilateral Thin Plate Bending Element," *International Journal for Numerical Methods in Engineering*, Vol. 18, 1982, pp. 1655–1677. doi:10.1002/nme.1620181106

[19] Beran, P. S., Strganac, T. W., Kim, K., and Nichkawde, C., "Studies of Store-Induced Limit-Cycle Oscillations Using a Model with Full System Nonlinearities," *Nonlinear Dynamics*, Vol. 37, 2004, pp. 323–339. doi:10.1023/B:NODY.0000045544.96418.bf

[20] Kerschen, G., Lee, Y. S., Vakakis, A. F., McFarland, D. M., and Bergman, L. A., "Irreversible Passive Energy Transfer in Coupled Oscillators with Essential Nonlinearity," *SIAM Journal on Applied Mathematics*, Vol. 66, No. 2, 2005, pp. 648–679. doi:10.1137/040613706

[21] Lee, Y. S., Kerschen, G., Vakakis, A. F., Panagopoulos, P., Bergman, L. A., and McFarland, D. M., "Complicated Dynamics of a Linear Oscillator with a Light, Essentially Nonlinear Attachment," *Physica D*, Vol. 204, Nos. 1–2, 2005, pp. 41–69. doi:10.1016/j.physd.2005.03.014